A Mathematical Model of Silicon Chemical Vapor Deposition

Further Refinements and the Effects of Thermal Diffusion

Michael E. Coltrin

Sandia National Laboratories, Albuquerque, New Mexico 87185

Robert J. Kee and James A. Miller

Sandia National Laboratories, Livermore, California 94550

ABSTRACT

We describe a mathematical model of the coupled gas-phase chemical kinetics and fluid mechanics in a chemical vapor deposition (CVD) reactor. This paper presents refinements to our earlier model of the CVD of silicon from silane. The model predicts gas-phase temperature and velocity fields, concentration fields for seventeen chemical species, and deposition rates. The major new features are a multicomponent transport model including thermal diffusion and a new formulation of the boundary conditions that describe deposition. A significant result is that thermal diffusion is predicted to make an important contribution to species density profiles and generally to reduce deposition rates.

Chemical vapor deposition (CVD) is used throughout the microelectronics industry to deposit thin films in the fabrication of integrated circuits. Despite the importance of CVD, there is little fundamental understanding of many of the deposition processes in use today. We are pursuing a course of research to describe the chemical and physical processes that occur in the gas phase during chemical vapor deposition.

Because CVD reactant gases are thermally unstable, they decompose in the presence of a heated susceptor, depositing a solid film. If the gas-phase decomposition rate is fast compared to the time for the reactant to diffuse to the heated surface, the molecule will decompose before reaching the surface. Gas-phase reaction rates in CVD are closely coupled to the temperature profile above the susceptor. Therefore, a model of the system must include gas velocity and temperature fields and the rates of chemical reactions in the CVD reactor.

We have previously presented such a mathematical model of the gas phase in the CVD of silicon from silane (1, 2). Our model is general in that it can be applied to other CVD systems for which a gas-phase kinetics mechanism is known. The silane CVD model predicts gas-phase temperature and velocity fields, concentration fields for 17 chemical species, deposition rates, and deposition uniformity as a function of experimental conditions such as susceptor temperature, flow rate, inlet partial pressure of silane, total pressure, and reactor dimension. We model reactors in which the gases flow along the length of a rectangular or cylindrical channel, depositing solid silicon on the reactor walls. Such a flow is reasonably modeled by the boundary layer equations.

This paper describes refinements we have made to the model since its original publication (1, 2). One important change is the inclusion of thermal diffusion, which is the separation of species of differing mass or size in a temperature gradient. Thermal diffusion can have an important effect on predicted concentration profiles. We have also introduced a more rigorous method of calculating multicomponent transport properties. The boundary condition describing chemical reactions at the surface has also been reformulated. The body of this paper is comprised of detailed discussions of the following topics: the equations defining our model, chemical reactions at the boundaries, the gas-phase mechanism, multicomponent transport, thermal diffusion, and numerical computation.

Description of Model

Defining equations.—As discussed before (1), we solve the boundary layer equations to describe the fluid flow. These equations are coupled to species conservation equations to describe chemical creation and destruction and both convective and diffusive transport. The applicability of these equations relies on the existence of a principal flow direction in which diffusive transport is negligible compared to convective transport. To simplify the numerical procedure, we recast the equations using the Von Mises transformation (3) in which the cross-stream coordinate is replaced by the stream function as an independent variable. In the past, we solved these equations on a fixed interval in stream function, which implies no net mass loss from the system. In cases where there is relatively little net mass loss due to deposition, this is a reasonable approximation, and the results of our previous work (1, 2) are not affected. However, in some cases, such as low pressure CVD, deposition reduces the mass flux significantly. We have introduced a further transformation and two new equations to account for the mass loss due to deposition at the upper and lower boundaries.

We first state the transformed set of equations describing our model and then discuss the transformation procedure itself.

Momentum

$$\rho u \frac{\partial u}{\partial x} - \rho u \frac{\xi}{M}\frac{dM}{dx}\frac{\partial u}{\partial \xi} + \frac{dp}{dx} = \frac{\rho u}{M^2}\frac{\partial}{\partial \xi}\left(\rho u \mu y^{2\alpha}\frac{\partial u}{\partial \xi}\right) + \rho g \qquad [1]$$

Species

$$\rho u \frac{\partial Y_k}{\partial x} - \rho u \frac{\xi}{M}\frac{dM}{dx}\frac{\partial Y_k}{\partial \xi} = \dot{\omega}_k W_k - \frac{\rho u}{M}\frac{\partial}{\partial \xi}(y^\alpha \rho Y_k V_{k_y})(k = 1, \ldots, K-1) \qquad [2]$$

Energy

$$\rho u c_p \frac{\partial T}{\partial x} - \rho u c_p \frac{\xi}{M}\frac{dM}{dx}\frac{\partial T}{\partial \xi} = \frac{\rho u}{M^2}\frac{\partial}{\partial \xi}\left(\rho u \lambda y^{2\alpha}\frac{\partial T}{\partial \xi}\right) - \sum_{k=1}^{K}\dot{\omega}_k W_k h_k - \frac{\rho^2 u y^\alpha}{M}\sum_{k=1}^{K} Y_k V_{k_y} c_{p_k}\frac{\partial T}{\partial \xi} \qquad [3]$$

State

$$p = \frac{\rho R T}{\bar{W}} \qquad [4]$$

In these equations, the diffusion velocity V_{k_y} is given by

$$V_{k_y} = \frac{\rho u y^\alpha}{X_k \overline{W} M} \sum_{j \neq k}^{K} W_j D_{kj} \frac{\partial X_j}{\partial \xi} - \frac{D_k^T}{\rho Y_k} \frac{\rho u y^\alpha}{TM} \frac{\partial T}{\partial \xi} \quad [5]$$

For an axisymmetric flow, the parameter α is 1 and y represents the radius measured from the reactor channel centerline. If α is zero, the equations are in planar coordinates and y is the height above the lower reactor wall. The independent variables x and ξ represent the axial coordinate (principal flow direction) and the normalized stream function, respectively. All variables are defined in the List of Symbols section at the end of the paper. The gravity term in the momentum equation is included only when gravity acts along the principal flow direction. Gravity is not included for the case of a horizontal reactor.

We define the stream function ψ in the normal way as

$$\psi = \int_0^y \rho u y^\alpha dy \quad [6]$$

The physical interpretation of the stream function is that there is a constant mass flow rate between two lines of constant stream function (*i.e.*, between streamlines when there is no mass loss from the system). If there is no mass loss, the reactor walls are also streamlines, *i.e.*, lines of constant stream function. The independent variable ψ then ranges from zero at one boundary to the total mass flow rate at the other. Under these conditions, the total mass flow rate is evaluated at the initial condition and is held constant throughout the computation. The numerical method uses a mesh in which each mesh point has a specified value of stream function. However, if mass is lost via deposition, then the total mass flow rate changes, and the independent variable ψ changes at each mesh point, *i.e.*, a moving coordinate system. In order to make a new independent variable that is fixed for the entire problem, we define a new stream function that is normalized by the local total mass flow rate M

$$\xi = \frac{\psi}{M} \quad [7]$$

Using this definition, ξ always ranges between 0 and 1, and the mesh in ξ remains fixed. In cylindrical coordinates, M is the total flow of mass past a point in the tube per unit radian per unit time. In planar coordinates, M is the mass flowing past a point in the tube per unit depth per unit time.

Equations [1]-[5] differ from those published in Ref. (1) by use of the normalized stream function ξ. The relationships between the physical coordinates (y and x) and the transformed coordinates (ξ and ψ) are stated in the following equations that define the transformation

$$\left(\frac{\partial}{\partial x}\right)_y = \left(\frac{\partial}{\partial x}\right)_\psi - \rho v y^\alpha \left(\frac{\partial}{\partial \psi}\right)_x$$

$$= \left[\left(\frac{\partial}{\partial x}\right)_\xi - \frac{\xi}{M}\frac{dM}{dx}\left(\frac{\partial}{\partial \xi}\right)_x\right] - \rho v y^\alpha \frac{1}{M}\left(\frac{\partial}{\partial \xi}\right)_x \quad [8]$$

$$\left(\frac{\partial}{\partial y}\right)_x = \rho u y^\alpha \left(\frac{\partial}{\partial \psi}\right)_x = \rho u y^\alpha \frac{1}{M}\left(\frac{\partial}{\partial \xi}\right)_x \quad [9]$$

The total flow rate is computed from an equation that accounts for the mass deposited on each boundary

$$\frac{dM}{dx} = \frac{dM_l}{dx} + \frac{dM_u}{dx} \quad [10]$$

The flow of gas into each boundary is a net convective velocity. In the next section we discuss calculation of reaction rates at the surface and the convective velocity v.

The rate at which mass is deposited at the lower boundary is determined from the convective mass flux to the boundary

$$\frac{dM_l}{dx} = -(\rho v)_l \quad [11]$$

Equation [11] applies only in the planar coordinate case, since, in axisymmetric coordinates, the lower boundary is the centerline, and thus there is no mass loss. The rate of mass loss at the upper boundary (which is the upper wall in planar coordinates or the outer radius in cylindrical coordinates) is similarly defined by

$$\frac{dM_u}{dx} = (\rho v y^\alpha)_u \quad [12]$$

The initial mass flow rate entering the channel is defined by

$$M_0 = \left(\int_0^{y_{max}} \rho u y^\alpha dy\right)_0 \quad [13]$$

which serves as the initial condition for Eq. [10].

The system of equations is completed by an equation that relates the cross-stream physical coordinate y to the normalized stream function

$$\frac{1}{M}\frac{\partial y^{\alpha+1}}{\partial \xi} = \frac{\alpha + 1}{\rho u} \quad [14]$$

This equation is simply a recasting of the stream function definition, Eq. [6].

The dependent variables of this parabolic system of differential equations are p, ρ, y^α, u, T, M, and Y_k. The system of equations that we actually solve in the numerical model are Eq. [1]-[4], [10], [14], and [15]. We use Eq. [2] for only $K - 1$ species. Equation [15] determines the Kth species (which is normally the carrier gas)

$$Y_k = 1 - \sum_{j \neq k}^{K} Y_j \quad [15]$$

We use Eq. [15] rather than solving for all K species from Eq. [2], because we have found that the numerical methods are more reliable using this formulation. Since the multicomponent transport model ensures that the mass fractions sum to one (or, equivalently, that the diffusive fluxes sum to zero), these two methods are formally equivalent, although they are numerically different.

At the initial conditions, *i.e.*, the entrance to the reactor channel, we specify profiles of u, T, and Y_k and the pressure. Typically, these are a fully developed parabolic velocity profile and a uniform mixture of silane and the carrier gas at room temperature. From the specified profiles, we compute the initial local flow rate M_0 and the physical locations of all the mesh points, *i.e.*, a profile of y^α.

The boundary conditions state that the velocity is zero at the walls and that the temperature matches a specified value. In the transformed equations, ξ is the independent variable and the physical coordinate y is a dependent variable. Therefore, we must specify as boundary conditions that $y = 0$ at the lower boundary and $y = y_{max}$ at the upper boundary (or channel radius in the axisymmetric case). Note that a boundary value of y is specified at both boundaries, even though Eq. [14] is only a first-order equation. This apparent overspecification is resolved by the fact that we retain the pressure as a dependent variable, although there is no explicit equation or boundary condition for p (1, 4). We determine the local pressure $p(x)$ that allows the two boundary conditions on y to be satisfied simultaneously. The pressure is uniform in the cross-stream direction as a consequence of the making the boundary layer approximations. The boundary conditions for chemical species concentrations involve deposition reactions, and they are discussed in some detail in the next section.

Reactions at the boundary.—Boundary conditions on the mass fraction of each species describe reactions at the surface. We define the probability that species k will react upon collision with the surface to be γ_k. The mass of

species k destroyed per unit area per unit time is derived from simple gas kinetic theory. It is the rate of collision of species k with the surface times the probability that k will react upon each collision times the mass of species k. A species Si_mH_n reacts to add m Si atoms to the surface and releases $n/2$ H_2 molecules into the gas stream. The total rate of mass loss from the system at a boundary is calculated from this collision model and is related to the convective velocity in the cross-stream direction by

$$(\rho v)_l = -\left(\sum_k \sqrt{\frac{k_B T}{2\pi W_k}}\, C_k \gamma_k W_{Si} \nu_{k,Si}\right)_l \qquad [16]$$

where $\nu_{k,Si}$ is a stoichiometric coefficient, the number of moles of Si solid formed when species k reacts at the surface. Equation [16] is written for the lower boundary. A similar equation applies at the upper boundary. This is the method used to calculate v needed in Eq. [11] and [12].

The boundary condition on each silicon containing species relates the chemical destruction rate of species k at the surface to the flux of k into the surface. The boundary condition (written for the lower boundary) is

$$(\rho Y_k v + \rho Y_k V_k)_l = -\left(\sqrt{\frac{k_B T}{2\pi W_k}}\, C_k \gamma_k W_k\right)_l \qquad [17]$$

For H_2, the boundary condition is that its mass flux away from the boundary balances the mass flux of silicon containing species to the boundary according to the equation

$$(\rho Y_{H_2} v + \rho Y_{H_2} V_{H_2})_l = \left(\sum_k \sqrt{\frac{k_B T}{2\pi W_k}}\, C_k \gamma_k W_{H_2} \nu_{k,H_2}\right)_l \qquad [18]$$

where the sum in Eq. [18] is over silicon containing species and ν_{k,H_2} is a stoichiometric coefficient, the number of moles of H_2 released when species k reacts at the surface. Note that summing Eq. [17] over all silicon containing species and adding Eq. [18] gives Eq. [16] for the convective velocity v and the required condition that the sum over all the diffusive fluxes is zero.

In our previous work (1, 2), the boundary condition used was that the diffusion velocity at the boundary equals the reaction probability times the diffusion velocity that would occur if the molecule reacted upon every collision with the surface. Equation [17] is conceptually clearer and easier to implement.

There is little experimental information on the surface reaction probabilities γ_k for species in the silane CVD system. As discussed in our earlier paper (1), we assume that the reactive intermediate species Si, SiH, SiH_2, SiH_3, Si_2, Si_2H_2, H_2SiSiH_2, H_3SiSiH, Si_2H_5, and Si_3, react with unit probability upon collision with the surface. Stable compounds are assumed to be relatively unreactive at the surface. In the absence of any experimental data, we set γ_k equal to zero for Si_2H_6 and Si_3H_8.

In our previous work (1), we used an Arrhenius surface reaction probability for SiH_4 derived from the experimental work of Farrow (5). In other experimental work, Joyce and co-workers (6-8) measured an exponential temperature dependence approximately equal to that of Ref. (5). However, their pre-exponential constant was roughly ten times smaller than observed by Farrow. In developing our present model using Eq. [17] as the deposition boundary condition, we found that using both the Farrow (5) and Joyce (6-8) values for γ_{SiH_4} yielded low temperature deposition rates that were much too large when compared with experiment (9).

Because there is at least a factor of ten uncertainty in the experimental value of γ_{SiH_4}, we have chosen to fit the pre-exponential constant to ensure that our model matches the experimental deposition rate (9) at low temperature in hydrogen carrier gas. Under these conditions, the gas-phase decomposition of SiH_4 should be slow relative to the reaction of SiH_4 on the surface. In fitting the parameter γ_{SiH_4}, we used the activation energy of Joyce *et al.* (8) and adjusted the pre-exponential constant to match the deposition rate measured by van den Brekel (9) at the lowest temperature reported (960 K). The deposition rate data in Ref. (9) are the only data available that provide enough information about experimental conditions (cell dimensions, flow velocity, reactant, and carrier gas partial pressures) for us to apply our model. However, other independent comparisons between our model predictions and experiment are made in Ref. (10). The Arrhenius expression obtained for the silane surface reaction probability is

$$\gamma_{SiH_4} = 5.37 \times 10^{-2} e^{-9400/T} \qquad [19]$$

where T is in degrees Kelvin.

In our earlier work (1), we included multiple reaction paths for the reaction of SiH_4 at the surface. However, because we are using a fit for the silane surface reaction probability, such detail is unwarranted.

Reaction mechanism.—Our model includes an elementary reaction mechanism for the thermal decomposition of SiH_4 and the subsequent reactions of intermediate species. The reaction mechanism and rate constants in Arrhenius form are given in Table I. Although the reaction mechanism is generally the same as published in our earlier work (1), some of the details have been refined. As discussed before (1), predictions of the model are relatively insensitive to the rate constants for all reactions except R-1. Therefore, mechanisms of deposition discussed in Ref. (1) remain unchanged by the present refinements.

Because the SiH_4 unimolecular decomposition is known to be in its pressure fall-off region at atmospheric pressures and below, we use the following form to explicitly treat the pressure dependence of this reaction

$$k_1 = (a + bP) A_1 T^{\beta_1} e^{-E_1/RT} \qquad [20]$$

where the constants A_1, β_1, and E_1 are listed in Table I, P is the total pressure in atmospheres, $a = 0.0504$, and $b = 0.9496$. This form for the rate constant was obtained by fitting the temperature and pressure dependence of the silane unimolecular decomposition rate constant obtained from an RRKM analysis (12) of the experimental data described in Ref. (11). We fit the pressure dependence of R-1 between 5 torr and 1 atm, the range over which we have applied our CVD model. This expression may not be valid at lower pressures. The nonstandard temperature dependence is included to account for curvature in an Arrhenius plot for R-1.

We have included three new species in the reaction mechanism: H_3SiSiH, H_2SiSiH_2, and Si_3H_8. References [13]-[15] discuss reactions of the two isomers of Si_2H_4. Our earlier model (1) did not distinguish between these two species. Reference (14) reports rate constants for reactions of trisilane. The new reactions for these species are R-10, R-16, R-17, R-25, R-26, and R-27.

Reaction R-2, loss of an H atom to form SiH_3, is much slower than reaction R-1. We find that reactions of species containing an odd number of hydrogen atoms do not play a very important role in the silane CVD system. Nevertheless, in order to model these species more accurately, we have included several new reactions in Table I, *i.e.*, R-6, R-11, R-12, R-13, R-20, and R-24.

Each of the reactions listed in Table I is reversible. Although not stated explicitly, all of the reactions in our earlier work (1) were also reversible. The rate constants for the reverse reactions can be obtained from the reaction thermochemistry. Thermochemical data for each species in the reaction mechanism are given in the Appendix.

Multicomponent transport.—We use a multicomponent transport model to calculate the diffusion velocity of Eq. [5]. Multicomponent viscosities, thermal conductivities, diffusion coefficients, and thermal diffusion coefficients are calculated as outlined by Dixon-Lewis (16). (We use the full multicomponent formulation rather than the more approximate Stefan-Maxwell formulation also discussed in Ref. (16).) These transport properties are evaluated numerically using a package of Fortran subroutines by Kee *et al.* (17).

Table I. Reaction mechanism

	Reaction	A[a]	β[a]	E[a]	Reference
R-1	$SiH_4 \leftrightarrow SiH_2 + H_2$[b]	2.54×10^{38}	−7.95	61.96	(11, 12)
R-2	$SiH_4 \leftrightarrow SiH_3 + H$	3.69×10^{15}	0	93	(11, 37)
R-3	$SiH_4 + SiH_2 \leftrightarrow Si_2H_6$	5.01×10^{12}	0	1.29	(38)
R-4	$SiH_4 + H \leftrightarrow SiH_3 + H_2$	1.04×10^{14}	0	2.5	(39, 40)
R-5	$SiH_4 + SiH_3 \leftrightarrow Si_2H_5 + H_2$	1.77×10^{12}	0	4.4	(37)
R-6	$SiH_4 + SiH \leftrightarrow Si_2H_5 + H_2$	1.45×10^{12}	0	2	(37)
R-7	$SiH_4 + SiH \leftrightarrow Si_2H_5$	1.43×10^{13}	0	2	(37, 41)
R-8	$SiH_4 + Si \leftrightarrow SiH_2 + SiH_2$	9.31×10^{12}	0	2	(37)
R-9	$Si + H_2 \leftrightarrow SiH_2$	1.15×10^{14}	0	2	(37)
R-10	$H_2SiSiH_2 \leftrightarrow SiH_2 + SiH_2$	1.00×10^{16}	0	59	(15)
R-11	$SiH_2 + H \leftrightarrow SiH + H_2$	1.39×10^{13}	0	2	(37)
R-12	$SiH_2 + H \leftrightarrow SiH_3$	3.81×10^{13}	0	2	(37)
R-13	$SiH_2 + SiH_3 \leftrightarrow Si_2H_5$	6.58×10^{12}	0	2	(37)
R-14	$SiH_2 + Si_2 \leftrightarrow Si_3 + H_2$	3.55×10^{11}	0	2	(37)
R-15	$SiH_2 + Si_3 \leftrightarrow Si_3H_2 + Si_2$	1.43×10^{11}	0	18.8	(37)
R-16	$H_2SiSiH_2 \leftrightarrow Si_2H_2 + H_2$	3.16×10^{14}	0	53	(13)
R-17	$Si_2H_6 \leftrightarrow H_2SiSiH_2 + H_2$	2.51×10^{14}	0	52.2	(15)
R-18	$H_2 + SiH \leftrightarrow SiH_3$	3.45×10^{13}	0	2	(37)
R-19	$H_2 + Si_2 \leftrightarrow Si_2H_2$	1.54×10^{13}	0	2	(37)
R-20	$H_2 + Si_2 \leftrightarrow SiH + SiH$	1.54×10^{13}	0	40	(37)
R-21	$H_2 + Si_3 \leftrightarrow Si + Si_2H_2$	9.79×10^{12}	0	42.6	(37)
R-22	$Si_2H_5 \leftrightarrow Si_2H_3 + H_2$	3.16×10^{14}	0	53	(37)
R-23	$Si_2H_2 + H \leftrightarrow Si_2H_3$	8.63×10^{14}	0	2	(37)
R-24	$H + Si_2 \leftrightarrow SiH + Si$	5.15×10^{13}	0	5.3	(37)
R-25	$Si_3H_8 \leftrightarrow Si_2H_6 + SiH_2$	4.90×10^{15}	0	52.99	(14)
R-26	$Si_3H_8 \leftrightarrow H_3SiSiH + SiH_4$	4.79×10^{14}	0	49.24	(14)
R-27	$H_3SiSiH \leftrightarrow H_2SiSiH_2$	6.31×10^{12}	0	29.2	(15)

[a] Arrhenius parameters for the rate constants in the forward direction written in the form $k = AT^{\beta} \exp(-E/RT)$. The units of A depend on the reaction order, but are given in terms of mols, cubic centimeters, and seconds. E is in kcal/mol. Rate constants for the reverse reactions can be calculated from the reaction thermochemistry.

[b] See text for discussion of the pressure dependence of reaction R-1.

In our previous work (1), we did not include the effect of thermal diffusion and used less rigorous "mixture-averaged" formulas (18) to calculate transport properties. These formulas are accurate in the limit that one component of the mixture is present in a great excess, and the formulas are exact for any binary mixture. In our application, the mixture-averaged transport coefficients require less than one-tenth the computer time to evaluate than the multicomponent properties. In most cases, the results predicted using the mixture-averaged transport coefficients are indistinguishable from those using the multicomponent model. However, in modeling low pressure CVD, where the carrier gas is not present in a great excess, or inlet mixtures that contain more than two large components (for example, a mixture of SiH_4, H_2, and a carrier gas), we find significant differences between the two transport models. For these cases, the more rigorous multicomponent transport model is required.

Although the mixture-averaged formulas are not adequate for all CVD applications, they are well suited to numerical computation. Therefore, we rewrite the multicomponent formulation, Eq. [5], in a form that recovers some desirable properties of the mixture-averaged form. The diffusion velocity using the mixture-averaged approximation is

$$V_{k_y} = -\frac{D_{k,m}\rho u y^{\alpha}}{X_k M}\frac{\partial X_k}{\partial \xi} - \frac{D_k^T}{\rho Y_k}\frac{\rho u y^{\alpha}}{TM}\frac{\partial T}{\partial \xi} \qquad [21]$$

The diffusion velocity of Eq. [21] depends explicitly on the concentration gradient of species k, whereas the multicomponent diffusion velocity of Eq. [5] depends on the concentration gradients of all the remaining species. As a result, the Jacobian of the diffusion velocity has a strong diagonal term in the former case, but not in the latter.

The numerical solution procedure is aided by using a new multicomponent diffusion coefficient, found by equating Eq. [5] and [21] and solving for $D_{k,m}$

$$D_{k,m} = \frac{\Sigma_{j \neq k}{}^{K} W_j D_{kj}(\partial X_j/\partial \xi)}{\overline{W}\Sigma_{j \neq k}{}^{K}(\partial X_j/\partial \xi)} \qquad [22]$$

The denominator in Eq. [22] is found by noting that

$$\frac{\partial X_k}{\partial \xi} = -\sum_{j \neq k}^{K} \frac{\partial X_j}{\partial \xi} \qquad [23]$$

This form of the denominator ensures that rounding errors are accumulated in roughly the same way in both the numerator and denominator. This method gives better numerical behavior in limiting cases, such as when a mixture approaches the limit of one pure species. We implement multicomponent transport using the diffusion velocity of the form in Eq. [21], with $D_{k,m}$ calculated using Eq. [22]. Note that we have made no approximations to the full multicomponent transport, but have simply rewritten the diffusion velocity in a form to aid numerical computation. Similar approaches to this problem have been discussed by Warnatz (19) and Dixon-Lewis (20).

Thermal diffusion.—Thermal diffusion is the separation of two species of differing mass and/or size in the presence of a temperature gradient. Because there are strong temperature gradients in a CVD reactor, thermal diffusion is expected to influence deposition rates (21, 22) as well as density profiles observed by *in situ* measurements (23-26). In order to make comparisons between predictions of our model and experimental density measurements (10), the effect of thermal diffusion is included in the diffusion velocity as the second term on the right side of Eq. [5].

Thermal diffusion significantly affects deposition rates and silane density profiles predicted by the model. We illustrate this with several sample calculations for the following conditions: 0.7 torr SiH_4 in 624 torr of carrier gas (either He or H_2), 5 cm cell height, 16 cm/s average flow velocity, and 4.5 cm from the leading edge of the susceptor. Figures 1-3 plot SiH_4 density as a function of height above the susceptor predicted by the model with and without thermal diffusion. Table II lists predicted deposition rates for the conditions in Fig. 1-3.

Three coupled effects lead to the general shape of the silane density curves in Fig. 1-3. The first, and simplest, effect is ideal gas expansion. The gas-phase temperature is highest at the susceptor, which causes a decrease in density near the susceptor. This expansion contributes significantly to all of the density profiles in Fig. 1-3. A second effect, gas-phase decomposition, also depletes the silane when the susceptor temperature is sufficiently high. Thermal diffusion is the third effect that contributes to the density profiles.

Figure 1 shows the silane density profile in helium carrier gas with a 550°C susceptor with (solid curve) and

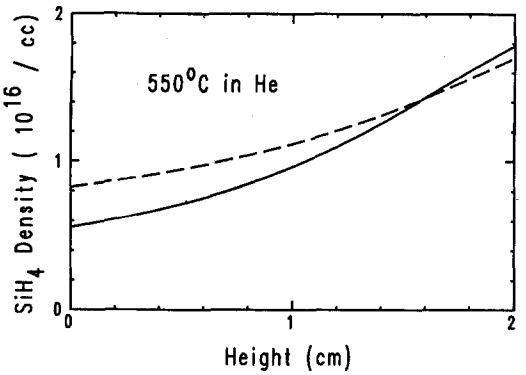

Fig. 1. Predicted SiH_4 density as a function of height above a 550°C susceptor in He carrier gas. The solid curve is calculated including thermal diffusion in the model, and the dashed curve is without thermal diffusion.

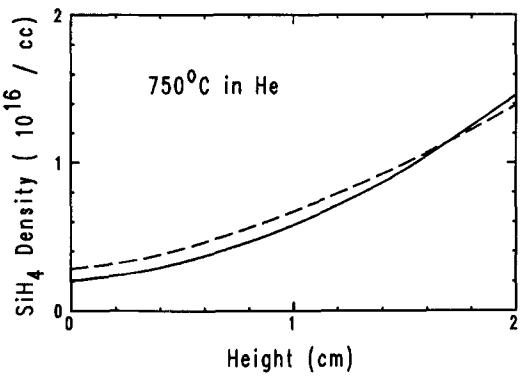

Fig. 2. Predicted SiH_4 density as a function of height above a 750°C susceptor in He carrier gas. The solid curve is calculated including thermal diffusion in the model, and the dashed curve is without thermal diffusion.

without (dashed curve) thermal diffusion. At this susceptor temperature, gas-phase and surface decomposition of silane are slow. When thermal diffusion is omitted from the calculation, the density profile is almost entirely due to expansion of the gas. The difference between the dashed and solid curves in Fig. 1 shows that thermal diffusion causes a substantial decrease in the silane density close to the susceptor.

The gas-phase pyrolysis of silane is much faster for the conditions illustrated in Fig. 2. Both expansion of the gas and gas-phase chemistry are very important for a 750°C susceptor in He carrier gas. Including thermal diffusion in the model has relatively less effect on the density profile than for the conditions of Fig. 1. Both the solid and dashed curves are shifted to much lower density for the 750°C susceptor, compared to the 550°C susceptor results.

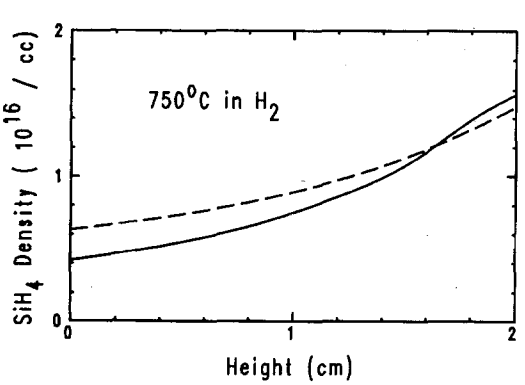

Fig. 3. Predicted SiH_4 density as a function of height above a 750°C susceptor in H_2 carrier gas. The solid curve is calculated including thermal diffusion in the model, and the dashed curve is without thermal diffusion.

Figure 3 shows how changing from He to H_2 carrier gas affects the silane density. Hydrogen is a product of the silane decomposition and suppresses the net decomposition. Therefore, gas-phase chemistry contributes less to the silane profile than in Fig. 2. As was the case in Fig. 1, thermal diffusion significantly decreases the predicted silane density above the susceptor.

Table II illustrates several features of the deposition rates predicted by the model. For each of the three sets of conditions described by Fig. 1-3, omitting thermal diffusion increases the deposition rate by approximately 50%. Increasing the susceptor from 550° to 750°C raises the deposition rate by about a factor of one hundred (an apparent activation energy of 40 kcal/mol). Changing from He to H_2 carrier gas decreases the deposition rate by a factor of ten. The high activation energy and strong carrier gas dependence of the deposition rate are well known for the silane CVD system (27).

Numerical computation.—We describe the numerical method in a previous paper (1), and Ref. (4) gives more detail about the implicit nature of the boundary conditions and the computation of the pressure drop. Nevertheless, we briefly outline the method here. The computational approach is a method of lines (MOL) in which the cross-stream spatial derivatives (ξ derivatives) are discretized by finite differences and the resulting system of ordinary differential equations (ODE) in the downstream direction x is solved by ODE software. However, unlike the ordinary MOL where the resulting system of ODE is in the standard form $y' = f(t, y)$, these equations are in a more general differential/algebraic equation (DAE) form $g(t, y, y') = 0$. In this notation, y and y' represent the components of the solution and their "time-like," or marching, derivatives (the x derivatives in the boundary layer equations), and t is "time-like," *i.e.*, x. The DAE's are solved by a computer code called DASSL (28), which is based on the backward differentiation formulas (BDF).

The BDF methods are implicit linear multistep methods that deal effectively with the stiffness that is common in chemical kinetics problems. An essential step in any implicit solution procedure is the formation of a Jacobian matrix, *i.e.*, the partial derivative of the residual g with respect to each component of the solution y. In solving these equations, one of the most expensive steps is evaluating the Jacobian, and computing the multicomponent transport properties is the most expensive part of the Jacobian evaluation. Therefore, large savings can be achieved if the Jacobian evaluation cost can be reduced. We find that this can be accomplished by holding the transport properties fixed when calculating the numerical Jacobian. Although this introduces some inaccuracy into the Jacobian, DASSL requires only an approximate Jacobian for the purpose of iterating to a converged solution (28). No error is introduced into the solution by making this simplification in the Jacobian, but the computer time is decreased by about a factor of ten.

Summary

We have described a number of improvements in our model (1, 2) of the coupled gas-phase fluid mechanics and chemical kinetics in a chemical vapor deposition reactor. The boundary layer equations were modified to account for mass-loss from the gas phase during deposition.

Table II. Effect of thermal diffusion on deposition rates

Susceptor temperature (°C)	Carrier gas	Deposition rate[a] with thermal diffusion	Deposition rate[a] without thermal diffusion
550	He	8.8×10^{-4}	1.3×10^{-3}
750	He	1.0×10^{-1}	1.5×10^{-1}
750	H_2	1.1×10^{-2}	1.7×10^{-2}

[a] Deposition rate in μm/min.

Table A-I. Polynomial coefficients for thermochemical data[a]

Molecule	a_1	a_2	a_3	a_4	a_5	a_6	a_7	Notes
SiH_4	0.14516E + 01	0.13987E − 01	−0.42345E − 05	−0.23606E − 08	0.13712E − 11	0.31134E + 04	0.12321E + 02	b
	0.79359E + 00	0.17671E − 01	−0.11398E − 04	0.35992E − 08	−0.45241E − 12	0.31982E + 04	0.15242E + 02	
SiH_3	0.25499E + 01	0.86278E − 02	−0.33388E − 05	0.22203E − 09	−0.42663E − 14	0.22939E + 05	0.90718E + 01	b
	0.17402E + 01	0.11720E − 01	−0.74227E − 05	0.23060E − 08	−0.28572E − 12	0.23075E + 05	0.12927E + 02	
SiH_2	0.41082E + 01	−0.23863E − 02	0.12247E − 04	−0.11841E − 07	0.37596E − 11	0.27981E + 05	0.17387E + 01	c
	0.20953E + 01	0.71013E − 02	−0.45661E − 05	0.14351E − 08	−0.17942E − 12	0.28284E + 05	0.11018E + 02	
SiH	0.38861E + 01	−0.30522E − 02	0.77163E − 05	−0.63374E − 08	0.18172E − 11	0.45066E + 05	0.71218E + 00	b
	0.25597E + 01	0.26834E − 02	−0.16510E − 05	0.49783E − 09	−0.59889E − 13	0.45277E + 05	0.69207E + 01	
Si	0.31793E + 01	−0.27646E − 02	0.44784E − 05	−0.32833E − 08	0.91213E − 12	0.53339E + 05	0.27273E + 01	d
	0.26506E + 01	−0.35763E − 03	0.29592E − 06	−0.72804E − 10	0.57963E − 14	0.53437E + 05	0.52204E + 01	
Si_2H_6	0.67347E + 00	0.40931E − 01	−0.44841E − 04	0.29952E − 07	−0.89010E − 11	0.79327E + 04	0.18627E + 02	e
	0.34074E + 01	0.27206E − 01	−0.17713E − 04	0.56391E − 08	−0.71378E − 12	0.75321E + 04	0.61321E + 01	
Si_2H_5	0.16579E + 01	0.35164E − 01	−0.42386E − 04	0.30819E − 07	−0.96428E − 11	0.26290E + 05	0.16755E + 02	e
	0.41460E + 01	0.21567E − 01	−0.13947E − 04	0.44143E − 08	−0.55597E − 12	0.25949E + 05	0.55824E + 01	
H_3SiSiH	0.28713E + 01	0.25015E − 01	−0.27840E − 04	0.19295E − 07	−0.59583E − 11	0.38601E + 05	0.11255E + 02	e
	0.43257E + 01	0.17127E − 01	−0.11168E − 04	0.35587E − 08	−0.45065E − 12	0.38399E + 05	0.47064E + 01	
H_2SiSiH_2	0.22401E + 01	0.31489E − 01	−0.44697E − 04	0.36202E − 07	−0.11911E − 10	0.27146E + 05	0.12424E + 02	e
	0.48581E + 01	0.15656E − 01	−0.98413E − 05	0.30398E − 08	−0.37497E − 12	0.26822E + 05	0.94805E + 00	
Si_2H_3	0.33467E + 01	0.21818E − 01	−0.30768E − 04	0.25126E − 07	−0.83826E − 11	0.51449E + 05	0.88449E + 01	e
	0.49947E + 01	0.11499E − 01	−0.73607E − 05	0.23082E − 08	−0.28832E − 12	0.51251E + 05	0.16770E + 01	
Si_2H_2	0.18611E + 01	0.12818E − 01	−0.27182E − 05	−0.71492E − 08	0.40687E − 11	0.40931E + 05	0.15300E + 02	e
	0.33488E + 01	0.11239E − 01	−0.81571E − 05	0.28228E − 08	−0.38140E − 12	0.40588E + 05	0.74527E + 01	
Si_2	0.29671E + 01	0.63119E − 02	−0.10970E − 04	0.89278E − 08	−0.27873E − 11	0.69870E + 05	0.92789E + 01	e
	0.41446E + 01	0.65234E − 03	−0.50108E − 06	0.18062E − 09	−0.25161E − 13	0.69694E + 05	0.38627E + 01	
Si_3H_8	0.77196E + 00	0.63442E − 01	−0.76726E − 04	0.54543E − 07	−0.16611E − 10	0.12071E + 05	0.21532E + 02	e
	0.60933E + 01	0.36580E − 01	−0.23892E − 04	0.76271E − 08	−0.96769E − 12	0.11297E + 05	−0.27475E + 01	
Si_3	0.45979E + 01	0.10715E − 01	−0.16100E − 04	0.10969E − 07	−0.27832E − 11	0.74766E + 05	0.34421E + 01	d
	0.74213E + 01	−0.11709E − 03	0.89820E − 07	0.71935E − 11	−0.25670E − 14	0.74146E + 05	−0.10365E + 02	
H	0.25000E + 01	0.00000E + 00	0.00000E + 00	0.00000E + 00	0.00000E + 00	0.25474E + 05	−0.45989E + 00	d
	0.25000E + 01	0.00000E + 00	0.00000E + 00	0.00000E + 00	0.00000E + 00	0.25474E + 05	−0.45989E + 00	
H_2	0.29432E + 01	0.34815E − 02	−0.77713E − 05	0.74997E − 08	−0.25203E − 11	−0.97695E + 03	−0.18186E + 01	d
	0.30558E + 01	0.59740E − 03	−0.16747E − 08	−0.21247E − 10	0.25195E − 14	−0.86168E + 03	−0.17207E + 01	
He	0.25000E + 01	0.00000E + 00	0.00000E + 00	0.00000E + 00	0.00000E + 00	−0.74537E + 03	0.91534E + 00	d
	0.25000E + 01	0.00000E + 00	0.00000E + 00	0.00000E + 00	0.00000E + 00	−0.74537E + 03	0.91534E + 00	

[a] See Eq. [A-1]-[A-3] for the relationships between the polynomial coefficients and thermochemical properties. For each molecule, the first row of coefficients is used for temperatures below 1000 K and the second row of coefficients is used above 1000 K.

[b] Fit to data in Ref. (31).

[c] Fit to data in Ref. (31), using ΔH_f taken from Ref. (33).

[d] Data from Ref. (30).

[e] Fit to data in Ref. (32).

A new set of boundary conditions for reactions of chemical species at the surface was introduced to describe deposition. A more rigorous multicomponent transport model was introduced, including the effect of thermal diffusion. We conclude that thermal diffusion makes an important contribution to calculated deposition rates and chemical species concentration profiles, generally reducing the predicted deposition rates.

Predictions of the model are compared elsewhere (10) with *in situ* measurements of chemical species densities and gas-phase temperatures. Results of our modeling support the importance of gas-phase chemistry in the silane CVD system.

Acknowledgments

We wish to thank L. R. Petzold and W. G. Breiland for many helpful discussions about this work. We also thank an anonymous reviewer for detecting an inconsistency in our original formulation of species boundary conditions. This work performed at Sandia National Laboratories and supported by the U.S. Department of Energy under contract No. DE-AC0476DP00789 for the Office of Basic Energy Sciences.

Manuscript submitted Sept. 18, 1985; revised manuscript received Jan. 21, 1986.

Sandia National Laboratories assisted in meeting the publication costs of this article.

APPENDIX
Properties of Chemical Species

Data on the thermochemistry of the chemical species are needed in order to calculate reverse rate constants for the reactions in Table I. In our computer model, all chemical reaction rates, thermochemical properties, and equation of state variables are evaluated by CHEMKIN (29), a general-purpose package of chemical kinetics Fortran subroutines. CHEMKIN requires polynomial fits to the temperature dependence of molecular heat capacities, enthalpies, and entropies. The form for these fits is (29, 30)

$$\frac{C_p}{R} = a_1 + a_2T + a_3T^2 + a_4T^3 + a_5T^4 \qquad [A\text{-}1]$$

$$\frac{H}{RT} = a_1 + \frac{a_2}{2}T + \frac{a_3}{3}T^2 + \frac{a_4}{4}T^3 + \frac{a_5}{5}T^4 + \frac{a_6}{T} \qquad [A\text{-}2]$$

$$\frac{S}{R} = a_1 \ln T + a_2T + \frac{a_3}{2}T^2 + \frac{a_4}{3}T^3 + \frac{a_5}{4}T^4 + a_7 \qquad [A\text{-}3]$$

where T is in degrees Kelvin.

A standard source for these polynomial coefficients is the NASA data base (30). However, for many of the silicon containing species, this data was not available. Ho *et al.* have recently reported heats of formation and harmonic vibrational frequencies for SiH_nCl_m species (31), Si_2H_n species (32), and Si_3H_8 (32). This work uses high quality *ab initio* electronic structure calculations combined with empirical correction factors to calculate thermochemical data. For most of the silicon containing species, we fit the temperature dependence of the data in Ref. (31) and (32) to obtain the polynomial coefficients of Eq. [A-1]-[A-3]. Table A-I gives the complete set of polynomial coefficients describing the thermochemical data that we use in our CVD model.

The enthalpies, entropies, and heat capacities obtained by evaluating the polynomial coefficients at 298 K are listed in Table A-II. The enthalpies for SiH_n compounds agree with the recommendations of Ho *et al.* (31) with the exception of SiH_2. Reference (31) obtains a value of 68.1 ± 3 kcal mol^{-1} for the enthalpy of SiH_2, which is much higher than the usually accepted value (33) of 58.0 kcal mol^{-1}. There has been additional recent evidence (34, 35) supporting an enthalpy greater than 58.0. However, the experimental rate constants used in our mechanism were obtained assuming the earlier value for the enthalpy of SiH_2. For consistency with the kinetics data we have used the value of 58.0 kcal mol^{-1} in our fits of the thermochemistry of SiH_2. The enthalpies for Si_2H_n species and Si_3H_8 agree with the results of Ho *et al.* (32), with the exception of Si_2H_2. We use an enthalpy of 83.5 kcal mol^{-1} for Si_2H_2, which was based on preliminary results of the work in Ref. (32). The final recommendation of Ho *et al.* (32) is 89.5 ± 5 kcal mol^{-1} for the enthalpy of Si_2H_2 at 298 K.

Table A-II. Thermochemical data for chemical species

Molecule	H_{298} (kcal mol^{-1})	S_{298} (cal mol^{-1} deg^{-1})	$C_{p\,298}$ (cal mol^{-1} deg^{-1})
SiH_4	8.2	48.8	10.3
SiH_3	47.8	51.7	9.6
SiH_2	58.0	49.4	8.3
SiH	91.7	44.2	7.0
Si	107.7	40.1	5.3
Si_2H_6	19.1	65.4	19.1
Si_2H_5	55.7	69.6	18.1
H_3SiSiH	80.2	67.5	16.5
H_2SiSiH_2	57.4	65.3	16.9
Si_2H_3	105.7	66.1	15.3
Si_2H_2	83.5	58.7	10.5
Si_2	141.0	54.9	8.1
Si_3H_8	28.9	83.2	28.2
Si_3	152.0	64.0	13.2
H	52.1	27.4	5.0
H_2	0.0	31.2	6.9
He	0.0	30.1	5.0

Table A-III. Potential parameters for chemical species

Molecule	σ(Å)	ϵ/κ (Kelvin)	Reference
SiH_4	4.084	207.6	(36)
SiH_3	3.943	170.3	(42)
SiH_2	3.803	133.1	(42)
SiH	3.662	95.8	(42)
Si	2.910	3036.0	(36)
Si_2H_6	4.828	301.3	(42)
Si_2H_5	4.717	306.9	(42)
H_3SiSiH	4.601	312.6	(42)
H_2SiSiH_2	4.601	312.6	(42)
Si_2H_3	4.494	318.2	(42)
Si_2H_2	4.383	323.8	(42)
Si_2	3.280	3036.0	(36)
Si_3H_8	5.562	331.2	(42)
Si_3	3.550	3036.0	(42)

Estimates of the intermolecular potentials for all of the species are needed in order to evaluate the transport properties. Table A-III lists Lennard-Jones parameters for the silicon containing species in our model. The potential parameters were available in the literature (36) for SiH_4, Si, and Si_2. Parameters for the remaining species were estimated, as outlined below.

Potential parameters for the species SiH, Si_2H_2, Si_2H_6, and Si_3H_8 were estimated by scaling to analogous carbon-containing species. For example, for SiH, we approximate

$$\epsilon_{SiH} = \epsilon_{CH} \times \frac{\epsilon_{SiH_4}}{\epsilon_{CH_4}} \qquad [A\text{-}4]$$

$$\sigma_{SiH} = \sigma_{CH} \times \frac{\sigma_{SiH_4}}{\sigma_{CH_4}} \qquad [A\text{-}5]$$

where the parameters for the carbon containing species were obtained from Ref. (36).

Potential parameters for SiH_2 and SiH_3 were obtained by linear interpolation between SiH and SiH_4

$$\sigma_{SiH_n} = \sigma_{SiH} + \frac{n-1}{3}(\sigma_{SiH_4} - \sigma_{SiH}) \qquad [A\text{-}6]$$

with a similar equation for ϵ. The potential parameters for Si_2H_3, H_3SiSiH, H_2SiSiH_2, and Si_2H_5 were obtained by linear interpolation between Si_2H_2 and Si_2H_6

$$\sigma_{Si_2H_n} = \sigma_{Si_2H_2} + \frac{n-2}{4}(\sigma_{Si_2H_6} - \sigma_{Si_2H_2}) \qquad [A\text{-}7]$$

with a similar equation for ϵ.

For Si_3, we estimate the cross section as in Ref. (36)

$$\sigma_{Si_3} = \frac{5}{12}(3 \times \sigma_{Si_2}) - 0.55 \qquad [A\text{-}8]$$

and approximate

$$\epsilon_{Si_3} = \epsilon_{Si_2} \quad [A\text{-}9]$$

LIST OF SYMBOLS

a_i	Polynomial coefficient for fits to thermochemical data
C_k	Molar concentration of the kth species
c_p	Mixture heat capacity
c_{pk}	Specific heat capacity of kth species
D_{kj}	Multicomponent diffusion coefficient
$D_{k,m}$	Mixture diffusion coefficient
D_k^T	Thermal diffusion coefficient
g	Acceleration of gravity
h_k	Specific enthalpy of kth species
K	Total number of species
k_B	Boltzmann's constant
M	Mass flow rate
M_l	Mass loss rate at the lower boundary
M_u	Mass loss rate at the upper boundary
M_0	Mass flow rate at the channel inlet
p	Thermodynamic pressure
R	Universal gas constant
T	Temperature
u	Fluid velocity in x direction
v	Fluid velocity in y direction
V_{ky}	Diffusion velocity of kth species
x	Distance along principal flow direction
X_k	Mole fraction of kth species
y	Cross-stream coordinate
y_{max}	Maximum channel dimension
Y_k	Mass fraction of the kth species
$\dot{\omega}_k$	Rate of production of kth species by chemical reaction
$\overline{W}$	Mixture mean molecular weight
W_k	Molecular weight of kth species
α	Coordinate index: 0 for planar, 1 for radial
ϵ	Lennard-Jones well depth
γ_k	Probability of reacting upon collision with the surface
λ	Mixture thermal conductivity
μ	Mixture viscosity
ν	Stoichiometric coefficient
ψ	Stream function
ρ	Density
σ	Lennard-Jones cross section
ξ	Normalized stream function

REFERENCES

1. M. E. Coltrin, R. J. Kee, and J. A. Miller, *This Journal*, **131,** 425 (1984).
2. M. E. Coltrin, R. J. Kee and J. A. Miller, in "Chemical Vapor Deposition," McD. Robinson, C. H. J. van den Brekel, G. W. Cullen, J. M. Blocher, and P. Rai-Choudhury, Editors, p. 31, The Electrochemical Society Softbound Proceedings Series, Pennington, NJ (1984).
3. See, for example, "Theory of Laminar Flows," Vol. IV, F. K. Moore, Editor, Princeton University Press, Princeton, NJ (1964); "High Speed Aerodynamics and Jet Propulsion," F. K. Moore, Editor, Princeton University Press, Princeton, NJ (1964).
4. R. J. Kee, L. R. Petzold, M. D. Smooke, and J. F. Grcar, in "Multiple Time Scales," Computational Techniques Series, J. U. Brackhill and B. I. Cohen, Editors, p. 113, Academic Press, San Diego (1985).
5. R. F. C. Farrow, *This Journal*, **121,** 899 (1974).
6. B. A. Joyce and R. R. Bradley, *Philos. Mag.*, **14,** 289 (1966).
7. G. R. Booker and B. A. Joyce, *ibid.*, **14,** 301 (1966).
8. B. A. Joyce, R. R. Bradley, and G. R. Booker, *ibid.*, **15,** 1167 (1967).
9. C. H. J. van den Brekel, Ph.D. Thesis, University of Nijmegen, Nijmegen, The Netherlands (1978).
10. W. G. Breiland, M. E. Coltrin, and P. Ho, *J. Appl. Phys.*, In press.
11. C. G. Newman, H. E. O'Neal, M. A. Ring, F. Leska, and N. Shipley, *Int. J. Chem. Kinet.*, **11,** 1167 (1979).
12. H. E. O'Neal, Personal communication. The Arrhenius factors are from an RRKM analysis of pressure dependence data described in Ref. (11).
13. J. Dzarnoski, S. F. Rickborn, H. E. O'Neal, and M. A. Ring, *Organometall.*, **1,** 1217 (1982).
14. A. J. Vanderwielen, M. A. Ring, and H. E. O'Neal, *J. Am. Chem. Soc.*, **97,** 993 (1975).
15. R. T. White, R. L. Espino-Rios, D. S. Rogers, M. A. Ring, and H. E. O'Neal, *Int. J. Chem. Kinet.*, **17,** 1029 (1985).
16. G. Dixon-Lewis, *Proc. R. Soc., London, Ser A*, **307,** 111 (1968).
17. R. J. Kee, G. Dixon-Lewis, J. Warnatz, M. E. Coltrin, and J. A. Miller, Sandia National Laboratories Report, In preparation (1986).
18. R. J. Kee, J. Warnatz, and J. A. Miller, Sandia National Laboratories Report, SAND 83-8209 (1983).
19. J. Warnatz, *Ber. Bunsenges. Phys. Chem.*, **82,** 193 (1978).
20. G. Dixon-Lewis, in "Combustion Chemistry," W. C. Gardiner, Editor, p. 21, Springer-Verlag, New York (1984).
21. J. P. Jenkinson and R. Pollard, *This Journal*, **131,** 2911 (1984).
22. J. Jůza and J. Cermák, *ibid.*, **129,** 1627 (1982).
23. W. G. Breiland and M. J. Kushner, *Appl. Phys. Lett.*, **42,** 395 (1983).
24. P. Ho and W. G. Breiland, *ibid.*, **43,** 125 (1983).
25. P. Ho and W. G. Breiland, *ibid.*, **44,** 51 (1984).
26. W. G. Breiland and P. Ho, in "Chemical Vapor Deposition," McD. Robinson, C. H. J. van den Brekel, G. W. Cullen, J. M. Blocher, and P. Rai-Choudhury, Editors, p. 44, The Electrochemical Society Softbound Proceedings Series, Pennington, NJ (1984).
27. W. A. Bryant, *Thin Solid Films*, **60,** 19 (1970).
28. L. R. Petzold, Sandia National Laboratories Report, SAND 82-8637 (1982).
29. R. J. Kee, J. A. Miller, and T. H. Jefferson, Sandia National Laboratories Report, SAND 80-8003 (1980).
30. S. Gordon and B. J. McBride, NASA Report, NASA SP-273 (1971).
31. P. Ho, M. E. Coltrin, J. S. Binkley, and C. F. Melius, *J. Phys. Chem.*, **89,** 4647 (1985).
32. P. Ho, M. E. Coltrin, J. S. Binkley, and C. F. Melius, *ibid.*, In press.
33. R. Walsh, *Acc. Chem. Res.*, **14,** 246 (1981).
34. J. A. Pople, B. T. Luke, M. J. Frisch, and J. S. Binkley, *J. Phys. Chem.*, **89,** 2198 (1985).
35. J. M. Jasinski, Submitted to *ibid.*
36. R. A. Svehla, NASA Report, NASA-TR 132 (1962).
37. Estimated. M. E. Coltrin and J. S. Binkley, Unpublished.
38. P. John and J. H. Purnell, *J. Chem. Soc.*, **69,** 1455 (1973).
39. E. R. Austin and F. W. Lampe, *J. Phys. Chem.*, **81,** 1134 (1977).
40. J. A. Cowfer, K. P. Lynch, and J. V. Michael, *ibid.*, **79,** 1139 (1975).
41. J. P. M. Schmitt, P. Gressier, M. Krishnan, G. DeRosny, and J. Perrin, *Chem. Phys.*, **84,** 281 (1984).
42. Estimated. See Appendix.